IEEE Access
Multidisciplinary ⋮ Rapid Review ⋮ Open Access Journal

Received 7 December 2023, accepted 3 January 2024, date of publication 19 January 2024, date of current version 26 January 2024.

Digital Object Identifier 10.1109/ACCESS.2024.3355946

RESEARCH ARTICLE

NeoCommLight: A Visible Light Communication System for RF-Restricted NICUs

G. D. HESHAN NIRANGA, ARYADEVI REMANIDEVI DEVIDAS, AND MANEESHA VINODINI RAMESH, (Senior Member, IEEE)
Center for Wireless Networks & Applications (WNA), Amrita Vishwa Vidyapeetham, Amritapuri, India
Corresponding author: Aryadevi Remanidevi Devidas (aryadevird@am.amrita.edu)

This work was supported in part by Amrita Vishwa Vidyapeetham.

ABSTRACT Visible Light Communication (VLC) is one of the emerging technologies of Optical Wireless Communications (OWCs) in finding sustainable solutions for the spectrum crunch of beyond 5G access technologies. This research work introduces the NeoCommLight system, a healthcare communication architecture for Neonatal Intensive Care Units (NICU) based on visible light communication, which offers a promising solution for RF-restricted areas and addresses the challenges posed by spectrum crunch and health concerns associated with traditional radio communication technologies. To demonstrate the feasibility and practicality of the proposed system, a prototype design is presented, accompanied by implementation details. Furthermore, the performance analysis of the NeoCommLight system is conducted, shedding light on crucial aspects such as communication delay, transmitter-to-receiver distance, variations in transmitter angle concerning the Line of Sight (LoS) axis, and the impact of diffraction caused by a knife edge obstacle placed between the transmitter and receiver. The performance analysis of the system showed that it could transmit data at a maximum data rate of 3 Mbps at a distance of 5 cm. The system could transmit data at a data rate 800 Kbps to a maximum distance of 2 meters.

INDEX TERMS Visible light communication (VLC), channel modeling, on-off keying (OOK), optical communication, photodiode (PD), optisystem, interference analysis.

I. INTRODUCTION

Wireless technology plays a crucial role in medical body area networks (MBANs), offering flexibility and convenience for both caregivers and patients. However, in certain hospital zones, the use of mobile phones and RF devices is restricted due to potential interference with medical devices and the harmful effects they may have on patients with implants and neonatal infants [1]. Particularly, newborn babies are highly vulnerable to even minimal amounts of RF radiation, making it necessary to find an alternative, eco-friendly communication solution for healthcare environments [2]. Additionally, conventional RF communication faces limitations in terms of spectrum availability for high data rate transmission.VLC has been successfully applied as an alternative for RF in various domains such as medical applications [3], [4], underwater communication, indoor positioning [5], [6], [7], [8], [9], and vehicle-to-vehicle communication [10]. VLC presents a promising solution for MBANs due to its wider bandwidth compared to RF and its non-harmful nature to humans [11].

However, when VLC is employed for medical applications, noise removal from the transmitted signal becomes a significant challenge [3], [14], [15], [16]. Biomedical signals, in particular, are difficult to detect due to their low amplitude [17]. Among the many modulation schemes that can be incorporated into VLC systems, On-Off Keying (OOK) modulation is one of the most widely used modulation schemes. The VLC system employs a microcontroller to encode data into bits and transmit it through blinking LEDs, utilizing OOK modulation [12]. A human being can discern the difference between modulated light and stable light with a frequency of up to 500 Hz [13]. The high-frequency blinking of LEDs is imperceptible to the human eye. A photodiode at the receiver detects the transmitted light, allowing the

The associate editor coordinating the review of this manuscript and approving it for publication was Jonathan Rodriguez.

microcontroller to decode the message. This emphasizes the need for a safer and more reliable communication technology in environments like hospitals, where RF restrictions are imposed. VLC offers several distinct advantages over RF systems, including an uncongested frequency spectrum and a wider bandwidth. This enables higher transmission rates and faster speeds for short-range communication, making it highly suitable for healthcare settings.

In this context, this paper proposes NeoCommLight, a VLC system designed for reliable data transmission of babies' vital signs in the Neonatal Intensive Care Unit to doctors' cell phones. The paper outlines the different blocks involved in the transmitter and receiver for establishing communication using visible light. It also presents various NeoCommLight architectures, considering factors such as cost-effectiveness and the number of neonatal units in the NICU. To ensure reliable data transmission, the interference analysis of the NeoCommLight system is performed, considering potential interferences induced by ambient light during transmission. Finally, a performance evaluation of the designed NeoCommLight system is conducted to assess its effectiveness. By addressing these aspects, this research work aims to contribute to the development of a robust VLC-based communication system for healthcare environments, specifically targeting the transmission of babies' vitals in the NICU to doctors' cell phones.

The rest of the paper is organized as follows: Section II discusses the related works. Section III describes the architectures and block diagram of the proposed NeoCommLight System. Section IV presents the interference modeling and analysis of the NeoCommLight System. Section V describes the implementation details of the NeoCommLight System.

II. RELATED WORKS

VLC has grabbed significant attention as a crucial technology for next-generation communication according to its dual functionalities, which include higher transmission rate and illumination. The LEDs have been used by visible light communication as access points (APs) to provide terminals with data service while drastically reducing costs. As part of this chapter, there is an overview of related works on fundamental principles, modulation techniques, channel modeling, applications, and challenges relating to VLC. This overview provides a comprehensive understanding of the underlying principles of VLC and the different modulation techniques used for its implementation. It also helps to understand the challenges and opportunities that can arise from the use of VLC in various applications.

Harald Haas, Liang Yin, and Cheng Chen et al. presented the indoor networking principles and challenges in visible light communication [8]. This article discusses why VLC is a beneficial technology, especially for sixth-generation (6G) cellular connections. In addition, the paper covers and discusses fundamental networking technologies like hybrid LiFi/Wi-Fi networking topologies and interference avoidance. Then the paper demonstrated that VLC is the best alternative approach for load balancing in indoor communication. Furthermore, they presented the software-defined networking (SDN) testbed deployment results in a real-world hybrid LiFi/Wi-Fi network. VLC/LiFi has been discovered to improve Wi-Fi networks by offloading data traffic drastically. This paper demonstrated that LiFi, in collaboration with Wi-Fi, can massively increase data density. The characteristics of VLC were not sufficiently mentioned in this paper. Our paper demonstrated the VLC characteristic graphs.

The VLC channel model based on Poisson stochastic network theory was explored by Qunzhen F and Hao Wu [18]. The paper is aimed to apply Poisson's stochastic network theory to produce a VLC channel model. Additionally, this publication unveiled their system's indoor LED light layout approach. This paper established simulation experiments with VLC theories. However, that paper does not simulate the noise distribution layout with distance. All noise distribution layouts in VLC architectures are covered in our research paper.

A journal article on detailed surveys and applications in hybrid RF/VLC systems was provided by Hisham Abuella, Mohammed Elamassie, Murat Uysal, et al. [19]. The user of this hybrid system could access either VLC or RF, or both. This article summarizes the latest innovations in hybrid RF/VLC systems, their advantages, and their limitations. Furthermore, it presented that the hybrid VLC/RF mechanism would be reduced RF interference and power allocation in the network. Next, they mentioned that network reliability would be increased under high user density and data rates by optimizing network power consumption, delay, and capacity. That paper said hybrid RF/VLC is more realistic for indoor communication when both RF and VLC subsystems exist.

Klaas M, Wesley Da Silva, Van der Z, and Marianne Pontara M, presented a patient monitoring system using Manchester-OOK visible light communication [20]. A low-cost, reliable VLC system was presented in this paper including real-world characterizations and experimental performance. This project focused on the transmission of the Manchester-based OOK signal, In such a proof-of-concept mechanism that makes use of the Eye Opening Penalty (EOP) metric. Here, factors such as line-of-sight link distance, modulation frequency, LED bias current, and signal pattern were evaluated. Also, Prototyped was successfully demonstrated in that project. That paper was not demonstrated the illuminance distribution according to the distance. Our paper clearly illustrated the illumination distribution graphs according to the given architectures.

Research on a demonstration-based hidden node problem in VLC networks was accomplished by Armin Makvandi, Yousef Seifi Kavian, and Ehsan Namjoo [21]. According to this statement, the authors suggested that the physical layer should have a receive to send/clear-to-send (RTS/CTS) mechanism to send and clear packets. As part of the study, they developed a prototype system (including five nodes) using ATmega128a microcontrollers, NRZ OOKS, and a star topology. There were very few costs associated with the

implementation of the system. In their research, they have developed a prototype system that is capable of archiving data rates up to 115.2 kbps. It was also examined whether the prototype RTS/CTS system results met the requirements of IEEE 802.15.7 standards. Using the RTS/CTS system, the results showed that the efficiency of the system increased by 300% and the data goodput by 300% as well as the average delay decreased by 50%, and the loss ratio decreased by 94%. However, the goodput values at the zeroth hidden node were much lower than those at the zeroth node of the IEEE 802.15.7 standard. Overall, there was a significant improvement in the performance of the RTS/CTS mechanism, as shown in the results graph that was shown as compared to the existing system. They completed their research with good results. This paper shows the simulated results.

An analysis of the performance of multi-user optical MIMO (Multiple Input-Multiple Output) for VLC research paper was presented by Mahesh Kumar and Navin Kumar [22], [23], [24], [25], [26]. As part of their study, they analyzed both the repetition coding (RC) and spatial modulation (SM) techniques to determine what bit error rate (BER) was induced. Based on the simulation results, it appears that spatial modulation offers better performance, especially at the lower end of the signal-to-noise ratio (SNR). However, it does not focus on the distribution of ambient noise inside the room when studying this analysis. Our paper provides a clear explanation of all the scenarios that can be used to distribute ambient noise.

A detailed study on the impact of multiple shadows on the VLC system was conducted by T Shang Qian Land Tang T [27]. It was found that shadowing is one of the significant barriers in the VLC network. In VLC channels, the blockage is one of the most crucial issues that need to be addressed. The researchers tried to present the impact that the shadow indoor VLC system has on the indoor environment. For their VLC indoor system, they developed mathematical expressions for the calculation of shadows in an accurate manner. They also consider the limitation of room size in the shadow reign. As part of the study, the effectiveness of the VLC system with shadow effect is analyzed in terms of performance metrics with respect to throughput and outages. Furthermore, the impact of multiple shadows on indoor VLC systems has also been investigated. As a result of their simulations, it was found that there was a correlation between throughput and optical power.

Based on the literature review conducted, it appears that no previous studies have proposed a VLC-based system specifically designed for NICU units to deal with the detrimental effects of RF radiation while also incorporating smart healthcare capabilities. Therefore, the contributions of the paper are summarized as follows:

1) A VLC-based communication architecture, NeoCommLight, for RF-restricted NICUs considering factors such as cost-effectiveness and the number of neonatal units in the NICU.
2) An interference model of NeoCommLight system and its simulation-based analysis.
3) Prototype implementation of NeoCommLight system.
4) Comprehensive analysis of NeoCommLight system concerning the crucial aspects such as communication delay, transmitter-to-receiver distance, variations in transmitter angle about the Line of Sight (LoS) axis, and the impact of diffraction caused by a knife edge obstacle placed between the transmitter and receiver. The results of these analyses give insights into the characteristics and capabilities of the NeoCommLight system.

III. NEOCOMMLIGHT SYSTEM: ARCHITECTURES AND BLOCK DIAGRAM

In the context of a NICU, the importance of an effective health monitoring system cannot be overstated. Premature or ill babies admitted to the NICU require continuous monitoring for their survival. In certain cases, the doctors must monitor the vital signs of babies from outside the NICU and provide recommendations to the healthcare personnel attending to them. By utilizing wireless communication technologies, doctors can remotely access and analyze the vital data of the babies, enabling them to make informed decisions and provide guidance to the on-site healthcare team [28], [29]. This remote monitoring capability allows for efficient healthcare management and timely interventions when required. The proposed system, NeoCommLight utilizes VLC as an alternative to RF technology, leveraging visible light for communication of vitals inside the NICU.

The selection of VLC technology in the NeoCommLight system design is particularly advantageous as it enables simultaneous illumination and communication capabilities. This capability significantly improves the overall quality of healthcare in NICUs by enabling seamless collaboration between doctors and on-site healthcare providers. It also reduces the need for doctors to be physically present in the NICU at all times, allowing them to monitor multiple patients simultaneously and allocate their expertise efficiently. Ultimately, the implementation of the NeoCommLight system in NICUs enhances patient care, facilitates faster response times, and supports better health outcomes for babies in critical care. In the design of the NeoComLight system, two architectures have been proposed to cater to cost-effectiveness and different environments within NICUs.

A. NEOCOMMLIGHT SYSTEM: ARCHITECTURES

Two distinct NeoCommLight architectures have been proposed for NICU areas, each offering a unique perspective. These architectural designs have been developed with flexibility in mind, ensuring that they can adapt to the evolving mobility requirements of incubators in the NICU environment. By utilizing VLC technology, NeoCommLight architectures provide an undependable wireless communication infrastructure within the NICU, thereby reducing the need for cumbersome and restrictive hard-wired

communication cables. The architecture 1 employs a different approach by employing a shared VLC transmitter to facilitate communication with multiple incubators. By using one transmitter and four receivers, this system optimizes cost and simplifies the overall communication setup. On the other hand, In architecture 2, a one-to-one VLC system is implemented, wherein each incubator unit is equipped with separate transmitter and receiver modules. The separate transmitter and receiver modules installed in each incubator unit enable direct and dedicated communication between the individual transmitter-receiver pairs. This setup offers a high degree of customization and privacy for each incubator, catering to specific patient needs and facilitating efficient communication between the healthcare personnel and the infants. In architecture 1, each receiver was assigned a unique identity code to reduce inter-module interference. A 4-bit code system was introduced before data transmission. The receivers then focused only on that code. If the code was successfully received, the receiver could decode the transmitted signal. Otherwise, the receiver would not be active for other codes.

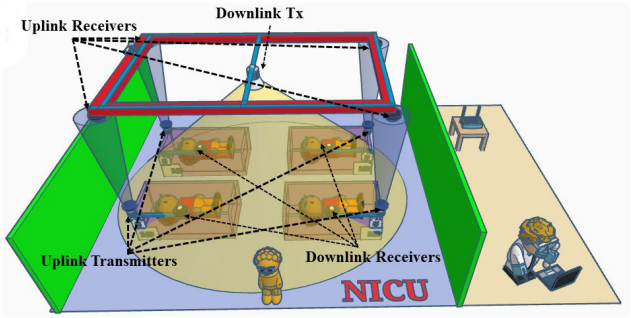

FIGURE 1. Architecture 1- Single transmitter and multiple receivers.

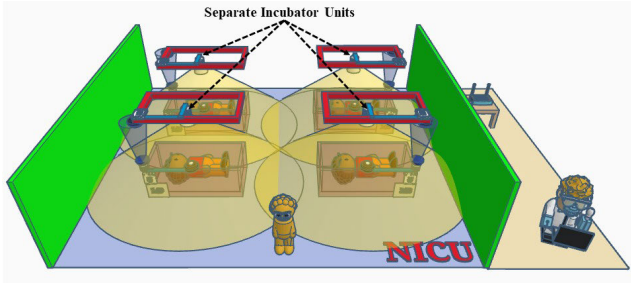

FIGURE 2. Architecture 2- one to one VLC connection.

The scenario depicted in Figure 1 showcases another NeoCommLight system architecture consisting of one transmitter and four receivers for the up-link and down-link communication in the NICU. This setup enables the doctor to access all incubators using a single high-power light source. Synchronization becomes crucial in this scenario to ensure smooth and reliable communication. To address the challenge of distinguishing data signals for each receiver, a 4-bit code is added before the actual data transmission. Each receiver waits for the specific 4-bit code assigned to them. Upon receiving the matching 4-bit code, the receiver detects and processes the subsequent data signal. If the transmitted 4 bits do not match the receiver's assigned code, the receiver continues to monitor the 4-bit code until a match is found. This mechanism ensures accurate and reliable data transmission and reception by the intended incubator units. To minimize interference in the up-link communication, specific separate time intervals are allocated for each incubator unit. This time division mechanism ensures that the transmissions from different units do not overlap, reducing the risk of signal interference and maintaining reliable communication.

Figure 2 illustrates the architecture of a one-to-one VLC system designed specifically for NICUs, where each incubator is equipped with a dedicated VLC transmitter and receiver. To optimize performance, the VLC transmitter is positioned in the corner of the incubator, taking advantage of the lower ambient noise levels in that area. Noise distribution simulations conducted in Matlab confirm that corner regions exhibit reduced noise compared to other spots. The down-link VLC system is represented by the yellow beam, while the up-link VLC system is depicted by the blue beam. The one-to-one communication design ensures a highly efficient transmission of information. However, it is important to note that implementing this architecture incurs a higher initial cost compared to alternative designs. Nevertheless, this cost is justified by the benefits it brings, including rapid decision-making and improved healthcare outcomes.

B. NEOCOMMLIGHT SYSTEM: BLOCK-DIAGRAM

The prototype of the NeoCommLight system comprises a Raspberry Pi module, photodiode, LCD, and healthcare monitoring sensors, providing comprehensive real-time monitoring of vital parameters, including heart rate, temperature, oxygen saturation, blood pressure, and other essential metrics. The Raspberry Pi module serves as the main processing unit, efficiently converting the measured parameters into binary data. These binary values are then transmitted to the LED driver circuit, where a high-power LED connected to the incubator emits the blinking visible light signals. In the receiving mode, the VLC receiving circuit captures the transmitted binary data and relays it to the Raspberry Pi module where the received signal is demodulated. The VLC module placed on the roof rail of the NeoCommLIght system consists of the Raspberry Pi module connected to a Wi-Fi router via high-speed Ethernet or fiber cables other than the LED and Photodiode circuitry. This allows doctors to access patient records seamlessly through the Internet. Doctors and administrators can remotely monitor each incubator from any location worldwide, facilitating timely and informed medical decisions. The doctors can provide specific instructions to the individual NICU units based on the received sensor parameters. The recommended instructions are promptly displayed on each unit's monitor, streamlining the workflow for nurses and promoting efficient implementation. The system's user-friendly interface, accessible through web and

mobile applications, allows doctors and administrators to access patient data, set instructions, and receive real-time updates effortlessly, even if they are not physically present in the NICU area. A block diagram in figure 3 shows the system modules for the two-way communication of the sensor values/vital parameters and the instructions from the incubator unit to the doctor outside the NICU area.

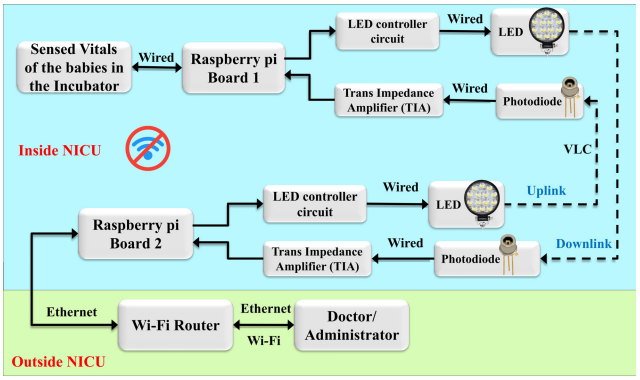

FIGURE 3. Detailed communication block diagram between sensed vitals of the incubator to the doctor/ administrator.

IV. VLC CHANNEL MODELLING OF NEOCOMMLIGHT SYSTEM AND ITS ANALYSIS

In this section, we present a comprehensive analysis of the optical power distribution [30], [31], [32] and noise distribution [33], [34], [35] about the line-of-sight (LOS) link within the NICU area. Realistic channel modeling and characterization are essential to ensure high quality-of-service (QoS) in communication systems. Our goal is to identify the optimal location coordinates of the VLC transceivers of the NeoCommLight system, for effective transmission of visible light signals, considering the two architectures explained in section III-A. For the VLC channel modelling and its analysis, we have considered the LED as the transmitter and the photodiode as the receiver. First, we modeled the channel and then analyzed the distribution of illuminance and noise using Matlab simulations. The simulations considered various critical variables, such as LED type, LED view angle, the number and positions of LEDs, receiving photodiodes' characteristics (responsivity, field of view - FOV, active area, and bandwidth), ambient noise, and other relevant parameters.

For the indoor VLC system, high-power LEDs are employed as the transmitter source, ensuring robust signal transmission. Additionally, large-area, high-sensitive photodiodes serve as receivers, optimizing the reception of VLC signals as shown in figure 4. In figure 4, Φ_{max} denotes the maximum radiation angle of the transmitting LED concerning the receiving Photodiode. The Φ and d represent the angle of irradiance and the distance between the illuminated surface and the illumination source. The field-of-view (FOV) angle of the photodiode based on its range of view is represented as Ψ_{FOV}.

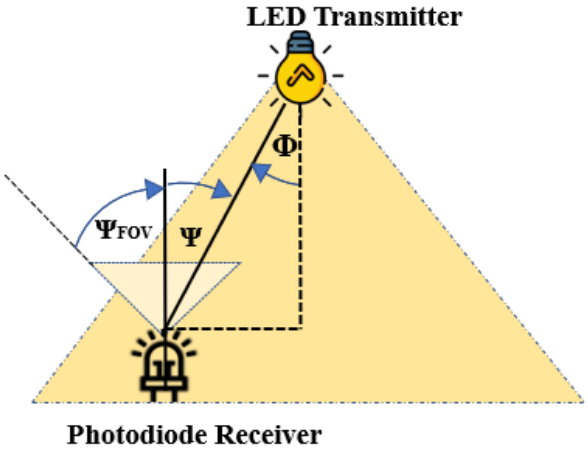

FIGURE 4. Geometry of line of sight (LOS) propagation model.

TABLE 1. Notations and descriptions.

Symbol	Parameter
Φ_{max}	Maximum radiation angle of the transmitting LED
Φ	Angle of irradiance of the transmitting LED
d	Distance between the illuminated Transmitter and Receiver
Ψ_{FOV}	Field-of-view (FOV) angle of the photodiode
Ψ	Incident angle
m	Lambert's mode number
$R_0(\Phi)$	Lambertian radiation intensity
$I_s(d, \Phi)$	Receiver irradiance
P_t	Average transmitted optical power
H_{LOS}	LOS channel direct current (DC) gain
A_r	Active area of the photodiode
T_s	Gain of an optical filter
P_{rp}	Received power in dB
σ^2_{total}	Total generated noise
σ^2_{shot}	Shot noise variance
$\sigma^2_{thermal}$	Thermal noise variance
$\sigma^2_{amplifier}$	Noise variance of the amplifier
σ^2_{dc}	Dark current noise
I_{bg}	Background current which is generated by the other ambient lights
q	Charge of the electron
B	Bandwidth of the photo-diode
I_2	Noise bandwidth factor
I_a	Amplifier's current
B_a	Amplifier's bandwidth
I_{dc}	Dark current
R	Photodetector responsivity

The radiation pattern of the LED optical transmitter is assumed to be Lambertian. Lambertian radiation intensity [33] distribution in Watt per Steradian (W/Sr) units is calculated based on the equation (1). Lambert's mode number m is responsible for the directional behavior of the LED source beam. The maximum power is radiated at the angle $\Phi = 0$.

$$R_0(\Phi) = \begin{cases} \dfrac{(m+1)}{2\pi} cos^m(\Phi) & -\pi/2 < \Phi < \pi/2 \\ 0 & \Phi > \pi/2 \end{cases} \quad (1)$$

The Lambertian order m [34] is correlated with the semi-radiation angle of the LED as shown in equation (2).

$$m = \frac{-ln(2)}{ln(cos(\Phi_{1/2}))} \tag{2}$$

The receiver irradiance, $I_s(d, \Phi)$ in Watts per Centimeter (W/cm) at d and ϕ is given in the equation (3), where P_t is the average transmitted optical power and d is the distance across transmitter (Tx) and receiver (Rx).

$$I_s(d, \Phi) = \frac{P_t R_0(\Phi)}{d^2} \tag{3}$$

In the NICU environment, VLC transmitting LEDs are strategically mounted on the ceiling, while photodiodes are precisely positioned on the incubator units, forming the receiving plane. In the NeoCommLight system, the line-of-sight (LOS) signals are exclusively focused to ensure direct and unobstructed communication. The LOS channel direct current (DC) gain [34], denoted by H_{LOS} as shown in equation (4), plays a pivotal role in determining the effectiveness of the LOS link. The received power distribution is expressed by equation (6), providing critical insights into the intensity of received VLC signals at different locations.

$$H_{LOS} = \begin{cases} \frac{A_r R_0(\Phi)}{d^2} T_s(\Psi) g(\Psi) cos(\Psi) & \Psi < \Psi_{FOV} \\ 0 & \Psi > \Psi_{FOV} \end{cases} \tag{4}$$

$$P_{rp} = H_{LOS} P_t \tag{5}$$

$$P_{rp}(dB) = 10log(P_{rp}) \tag{6}$$

In the given equation, $\phi = 0$ represents the angle of maximum radiated power for the VLC system. The variables, A_r refer to the active area of the photodiode (PD), d denotes the LOS distance between the PD and the LED, and T_s represents the gain of an optical filter, hold crucial significance. These variables collectively contribute to determining the efficiency and performance of the LOS link in the VLC system, aiding in improved signal reception and transmission.

In the context of indoor VLC systems, it is crucial to comprehend the impact of noise on the VLC Line-of-Sight (LOS) channel model. The noise in such systems originates from various sources, which include dark current [36], thermal noise [32], amplifier noise [35], and shot noise [32]. Each of these sources contributes to the overall noise generated by the indoor VLC system. To quantify the total noise generated, σ^2_{total}, by the system, we have used the below equation,

$$\sigma^2_{total} = \sigma^2_{shot} + \sigma^2_{thermal} + \sigma^2_{amplifier} + \sigma^2_{dc} \tag{7}$$

$$\sigma^2_{total}(dB) = 10log(\sigma^2_{total}) \tag{8}$$

In the equation (7), σ^2_{shot} represents the shot noise variance. The symbol $\sigma^2_{thermal}$ corresponds to the thermal noise variance and the $\sigma^2_{amplifier}$ represents the noise variance of the amplifier. Finally, the dark current noise is denoted by the σ^2_{dc}. The variance of shot noise [32] is given in the equation (9).

$$\sigma^2_{shot} = 2qRBP_{rp} + 2qBI_{bg}I_2 \tag{9}$$

It is very crucial to find out the impact of ambient lights on the photodiode to determine the interference it is posing to the actual visible light communication. The background current generated by the other ambient lights is denoted by I_{bg} as in equation (9). The q represents the charge of the electron and the B denotes the bandwidth of the photo-diode. The noise bandwidth factor, denoted by the I_2, is typically equal to 0.562 [32]. The equation (10) allows us to determine the variance of amplifier noise [35], $\sigma^2_{amplifier}$. The symbol I_a represents the amplifier's current, and B_a denotes the amplifier's bandwidth.

$$\sigma^2_{amplifier} = I_a^2 B_a^2 \tag{10}$$

$$\sigma^2_{dc} = 2qBI_{dc} \tag{11}$$

The dark current noise variance [36] is represented by σ^2_{dc} as shown in the equation (11). The I_{dc} represents the dark current, a small amount of electric current generated even in the absence of light. Signal-to-noise ratio (SNR) measures the useful information in a noisy environment. In equation (12), the SNR is expressed as a function of the photodetector responsivity R, received optical power, and noise variance [32].

$$SNR = \frac{(RP_{rp})^2}{\sigma^2_{total}} \tag{12}$$

This study utilizes the equations from (1) to (12) to comprehensively analyze each architecture of the designed system. By applying these equations, the research can effectively determine the number of VLC transmitters required in any VLC-accessible area, based on the analysis of received power distribution and noise power distribution.

A. ANALYSIS OF RECEIVED POWER DISTRIBUTION FOR ARCHITECTURE 1: SINGLE VLC LED TRANSMITTER

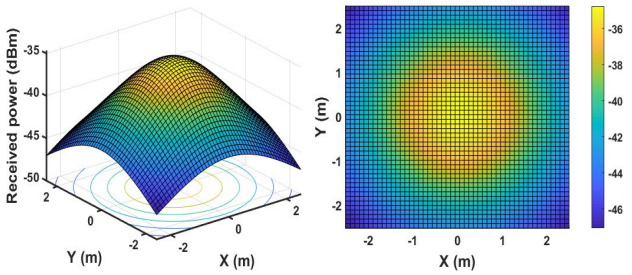

FIGURE 5. Received power distribution (dBm) for architecture 1(One Tx).

To evaluate the distribution of received power for architecture 1 in figure 1, which comprises of one LED transmitter and four downlink receivers, simulations were conducted using Matlab. The received power distribution is exhibited in the figure 5. The LED was placed in the center of the ceiling in this configuration. This resulted in stronger signal reception

in the middle and gradually weakening towards the corners. Based on this observation, it may be beneficial to consider placing the VLC receivers closer to the center of the room to potentially improve performance. As a result, the receivers may experience increased received power levels which can lead to improved overall performance. The table 2 outlines the simulation parameters used in the Matlab simulations for architecture 1.

TABLE 2. System parameters for received power distribution analysis of the VLC architecture 1.

Parameters	Values
Room size	$5 \times 5 \times 3m^3$
Power of the LED	42W
LED coordinates	2.5,2.5,3
Semi angle of the LED (Φ)	60^0
Receive plane above the floor	1m
Active area (AR)	$0.01m^2$
Field of view of PD Ψ_{FOV}	70^0
Gain of an optical filter (Ts)	1
Non imaging concentrator gain(g)	1

B. ANALYSIS OF RECEIVED POWER AND NOISE DISTRIBUTION FOR ARCHITECTURE 2: TWO VLC TRANSMITTERS

One case of architecture 2, employing two VLC transmitters and two VLC receivers, stands as a more reliable solution than architecture 1. A notable advantage of this design is its inherent redundancy: in the event of a malfunction in one downlink VLC transmitter, the other VLC downlink transmitter can still access both VLC receivers. To analyze the power distribution, MATLAB was used, employing the equations described above to plot the received power distribution graph. Despite having only two light beams, the design demonstrates high received power distribution under LED transmitters. Integrating the separate power distribution statements for Light 1 and Light 2 enables the plotting of the final power distribution graph for the receiving plane in the room, represented in figure 6. The system parameters used in the MATLAB simulation for architecture 2 are provided in Table 3. This comprehensive approach ensures an insightful evaluation of the system's performance and aids in optimizing the VLC network for efficient communication.

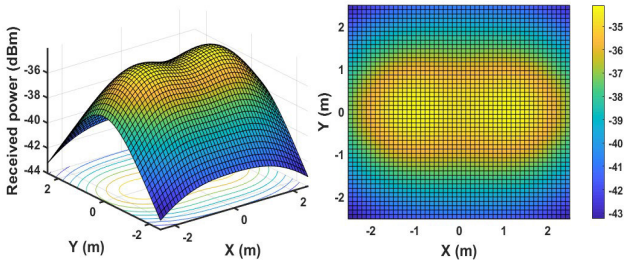

FIGURE 6. Received power distribution (dBm) for one case of architecture 2 (Two Tx).

TABLE 3. System parameters of one case of VLC architecture 2.

Parameters	Values
Room size	$5 \times 5 \times 3m^3$
Power of the LED	42W
LED 1 coordinates	-1,0,3
LED 2 coordinates	1,0,3
Semi angle of the LED (Φ)	60^0
Receive plane above the floor	1m
Active area (AR)	$0.01m^2$
Field of view of PD Ψ_{FOV}	70^0
Gain of an optical filter (Ts)	1
Non imaging concentrator gain(g)	1
Charge of an electron(q)	$1.60217663 \times 10^{-19}$
Bandwidth of the Photodiode (B)	1 GHz
Responsivity of the Photodiode(R)	0.47
Dark current of the photodiode I_{dc}	0.1nA
Amplifier current noiseI_a [36]	$3.7pA\sqrt{Hz}$
Amplifier bandwidth B_a	90MHz

In this particular case of architecture 2, the communication involves two VLC LED transmitters, and it is vital to take into account the influence of ambient noise sources on the communication link. When VLC transmitter 1 communicates with receiver 1, VLC transmitter 2 becomes an ambient noise source that can potentially affect the signal reception. To assess the impact of this ambient noise, the noise distribution equation (8) was employed in MATLAB, enabling the plotting of the noise distribution graph represented in figure 7. During the communication between VLC transmitter 1 and receiver 1, it is essential to consider all other light sources present in the environment as ambient noise, including VLC transmitter 2. Accurate analysis and visualization of the noise distribution provide valuable insights into the system's performance and its susceptibility to interference from ambient sources. By understanding the noise distribution, engineers and designers can optimize the VLC system's parameters and configuration, ultimately enhancing its reliability and efficiency in real-world scenarios.

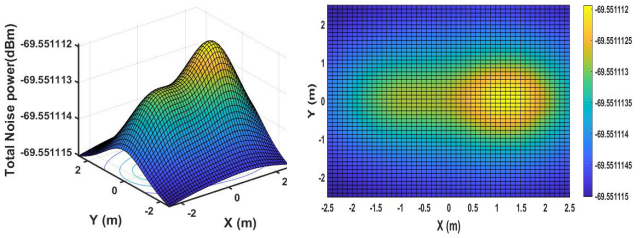

FIGURE 7. Noise power distribution (dBm) for VLC receiver 1 (Rx1) for a case of architecture 2 (Two Tx).

C. ANALYSIS OF RECEIVED POWER AND NOISE DISTRIBUTION FOR ARCHITECTURE 2: FOUR VLC TRANSMITTERS

In figure 2, architecture 2 is depicted, featuring four LED transmitters and four separate receivers. The four LED transmitters generate distinct light beams that overlap, resulting in the consideration of ambient noise as a critical

factor in VLC communication. To evaluate the performance of architecture 2, the equation for received power distribution, (8), was employed to plot the received power distribution graph using Matlab as shown in figure 8. Additionally, the noise power distribution graph was plotted as given in figure 9 based on the system parameters of VLC architecture 2 as shown in table 4. During the analysis, it was observed that the received power on the receiving plane was notably high under each transmitter location. The objective was to identify areas with reduced noise and high received power to ensure reliable communication. Based on the received power and noise distributions, the VLC receivers were positioned in the corner areas of the incubators. By strategically selecting receiver locations, engineers can enhance the signal-to-noise ratio, resulting in improved communication performance and increased overall efficiency of the VLC system in this configuration.

TABLE 4. System parameters of the VLC architecture 2.

Parameters	Values
Room size	$5 \times 5 \times 3m^3$
Power of the LED	42W
LED 1 coordinates	-1.25,-1.25,3
LED 2 coordinates	1.25,-1.25,3
LED 3 coordinates	-1.25,1.25,3
LED 4 coordinates	1.25,1.25,3
Semi angle of the LED (Φ)	60^0
Receive plane above the floor	1m
Active area (AR)	$0.01m^2$
Field of view of PD Ψ_{FOV}	70^0
Gain of an optical filter (Ts)	1
Non imaging concentrator gain(g)	1
Charge of an electron(q)	$1.60217663 \times 10^{-19}$
Bandwidth of the Photodiode (B)	1 GHz
Responsivity of the Photodiode(R)	0.47
Dark current of the photodiode I_{dc}	0.1nA
Amplifier current noiseI_a [36]	$3.7pA\sqrt{Hz}$
Amplifier bandwidth B_a	90MHz

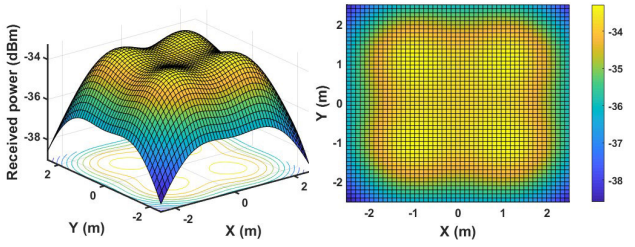

FIGURE 8. Received power distribution (dBm) for architecture 2 (four Tx).

In incubator 1 of architecture 2, where VLC transmitter (Tx 1) and receiver (Rx 1) are in communication, light from all other three LED transmitters in the system is considered ambient noise. The noise power distribution graph was plotted using equation (8), which takes into account shot noise, amplifier noise, dark current noise, and background noise. Shot noise, represented by equation (9), is influenced by the received power on the plane. As a result, the noisy power distribution during the communication between VLC transmitter 1 and receiver 1 depends on the combination of the received power distribution due to the VLC transmitters 2, 3, and 4. To optimize the placement of VLC receivers, the location coordinates of receiver 1 were set to $(-1.25, -1.25, 0)$, resulting in low noise and high received power at that position. Following this approach, all other VLC receivers were strategically placed at the outer corners of each incubator within architecture 2. This systematic arrangement of receivers aims to maximize signal quality and minimize interference from ambient noise sources, ultimately enhancing the performance and reliability of the VLC system in incubator 1.

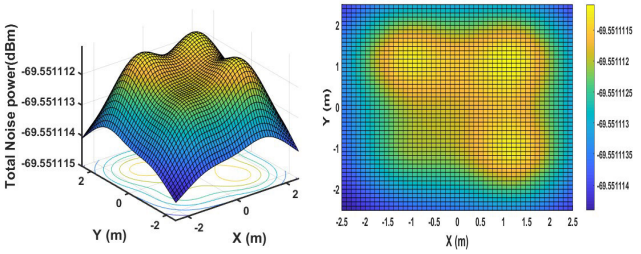

FIGURE 9. Noise power distribution (dBm) for Rx 1 in architecture 2.

D. VLC INTERFERENCE ANALYSIS USING OPTISYSTEM

The Matlab simulation results presented in the previous section gave the position of the VLC receivers to achieve high signal quality and less noise. In this section, we analyze the interference of the VLC communication, if the VLC transmitters and receivers were positioned on the location coordinates as given in figure 10 using the Optisystem simulation tool. Using OptiSystem software, we have been able to design, test, and simulate a free space optical communication (FSO) link in VLC [37], [38]. Free-space optical communication (FSO) is a method of wireless communication in which data is transmitted and received using light in free space. For systems with inter-symbol interference and noise, OptiSystem quantifies characteristics like BER (Bit Error Rate) and Q-Factor using numerical investigations and semi-analytical approaches to determine whether the VLC system is maximizing its performance.

According to the architecture shown in figure 10, Tx1 & Rx1 is one communication link, and Tx2 & Rx2 is another communication link. If we consider the VLC communication between Tx1 and Rx1, the light from Tx2 will be the ambient noise. Similarly, if we consider the communication between Tx2 and Rx2, the light from Tx1 will be ambient noise. The parameters of the photodiode [39] and trans-impedance amplifier (TIA) [40] in the Optisystem model are selected according to the photodiode and TIA used in the implementation of the NeoCommLight system. Table 5 shows all the parameters used in this Optisystem simulation.

The FSOL (Free Space Optical Link) is composed of the following key components: the optical transmitter (LED),

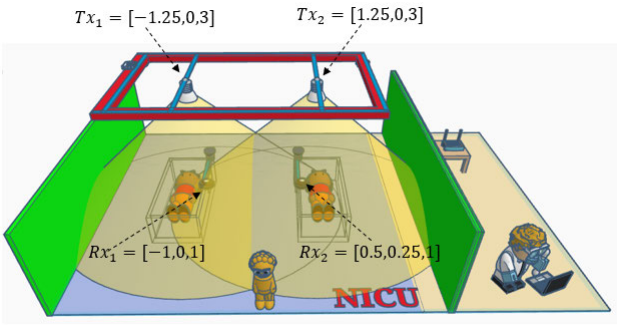

FIGURE 10. Architecture 2: with location coordinates of transmitters and receivers.

TABLE 5. Optisystem component parameters.

Parameters	Values
Input power of Tx1 and Tx2	42W
Semi angle of the LED (Φ)	60^0
lamberts number (m)	1
LED frequency	125GHz
Modulation type	NRZ
Gain of the amplifier(TIA)	90MHz
Amplifier current noiseI_a [35]	$3.7pA\sqrt{Hz}$
Photodiode Type	Silicon
Effective area of the photodiode	$0.5mm^2$
Responsivity of the photodiode	0.47W/A
Dark current of the photodiode	0.1nA
Receiver Aperture diameter	1cm
Distance between TX1 and RX1	2.015564m
Distance between TX2 and RX2	2.150581m
Distance between TX1 and RX2	2.66926956301m
Distance between TX2 and RX1	3.0103989447m
Angle between Tx2 and Rx1 (Φ_1)	48.36646^0
Angle between Tx1 and Rx2 (Φ_2)	41.47293^0
Received power of Rx1 because of Tx2 (P_{RX1})	$3.2566 \times 10^{-7}W$
Received power of Rx2 because of Tx1 (P_{RX2})	$5.2657 \times 10^{-7}W$

FSO link, optical amplifier, optical receiver (photodetector), demodulator, low pass filter, and BER analyzer. The optical transmitter, typically an LED, modulates data into optical signals, and these signals are transmitted through the Free Space Optical (FSO) link, enabling the wireless transmission of data optically across a medium. To ensure reliable and efficient data reception, the optical amplifier is employed to amplify the optical data within the FSO channel, making it easily detectable by the optical receiver (photodetector). The photodetector, typically a photodiode, captures the incoming optical signal and converts it into an electrical current signal, allowing further processing of the received data. After demodulation, where the original data is electronically retrieved from the carrier wave, the signal requires filtering to remove any unwanted noise or artifacts. As the final step, the Bit Error Rate (BER) analyzer analyzes the recovered signals and determines the bit error rate (BER), which quantifies the accuracy of the received data. The BER analyzer also displays the resulting signal, including an eye diagram, which provides insights into the signal quality and helps optimize the overall performance of the NeoCommLight system.

E. OPTISYSTEM MODEL: SUMMARY AND RESULTS

The architecture 2 of the NeoCommLight system is designed using Optisystem 20, with a simulation setup illustrated in figure 11. The data is transformed into non-return-to-zero (NRZ) electrical pulses using a pseudo-random data sequence, and an instantaneous white light is generated from the LED. The high-power white LED emits the modulated output with an optical power of 42 W. The communication link is established over free space between the high-power white LED and the receiving silicon photodiode at room temperature. The VLC channel employs free space optics, and its characteristics are determined based on experimental observations, considering only the Line of Sight (LOS) model. Measured FSO parameters are calculated using this LOS model. In this setup, ambient light from all other sources is assumed, as interference or noise during communication between VLC transmitter 1 (Tx1) and VLC receiver 1 (Rx1). Similarly, LED transmitter 2 (Tx2) acts as ambient noise when VLC receiver 1 and transmitter 1 communicate. The received power of Receiver 1 (P_{RX1}) because of the VLC transmitter 2 (Tx2) was calculated. Also, the received power of Receiver 2 (P_{RX2}) because of the VLC transmitter 1 (Tx1) is calculated using the equations. It was added to the photodiode as a separate white LED source using an optical coupler. The ambient light is merged with the modulated white LED signal using an optical coupler before the FSO transmission link.

The eye diagram serves as a valuable tool for assessing signal transmission quality, effectively summarizing the effects of Inter-Symbol Interference (ISI) by displaying the responses of 0's and 1's in the received signal. By overlapping plots of the received signal for every symbol time, the eye diagram provides insights into the ISI and eye-opening, representing the quality of the signal. The maximum width of the opening eye represents the best sampling time. In this context, the eye diagram in figure 12 was generated for VLC Receiver 1 (Rx1) position. The eye diagram in figure 13 was generated for VLC Receiver 2 (Rx2) position. The diagrams include merged light and noise signals, showcasing the received signal quality of Rx1 and RX2 in this simulation. According to the location coordinates of Tx1, Rx1, Tx2, Rx2 in the architecture in figure 10 and as per the system parameters in table 5, the distance between Tx1 and Rx1 is shorter compared to the distance between Tx2 and Rx2. Consequently, the received power at Rx1 is higher than at Rx2. Furthermore, the theoretical noise power at Rx1 is expected to be lower than at Rx2 due to the greater distance between Tx2 and Rx1. As a result, Rx1 exhibits better performance compared to Rx2. This observation is further validated by the eye diagram for Rx1, displaying a larger eye-opening size and indicating a higher signal-to-noise ratio (SNR). The quality factor (Q-factor), which represents the SNR's quality in the ''eye'' of the optical

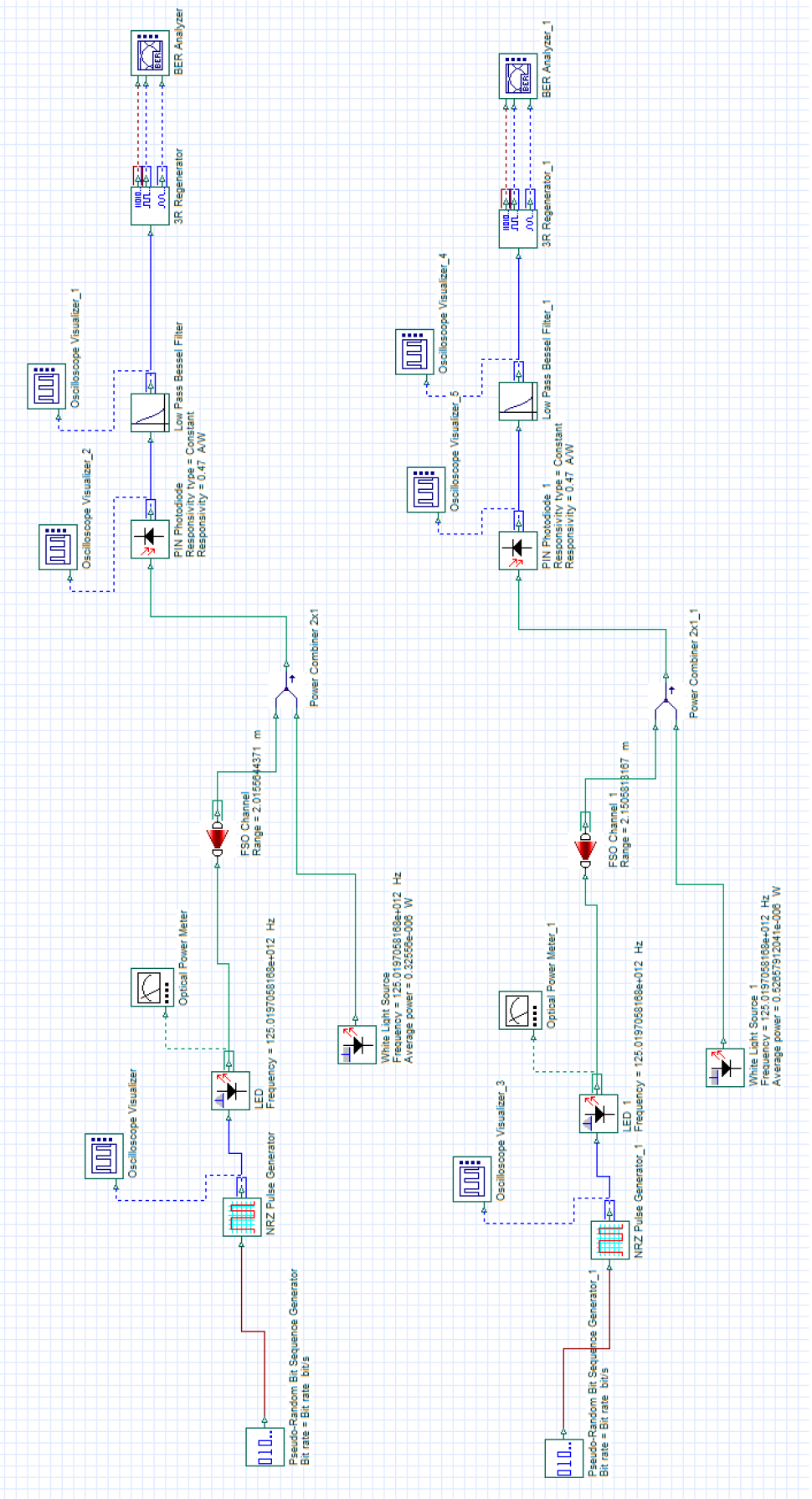

FIGURE 11. Optisystem designed block for VLC architecture 3.

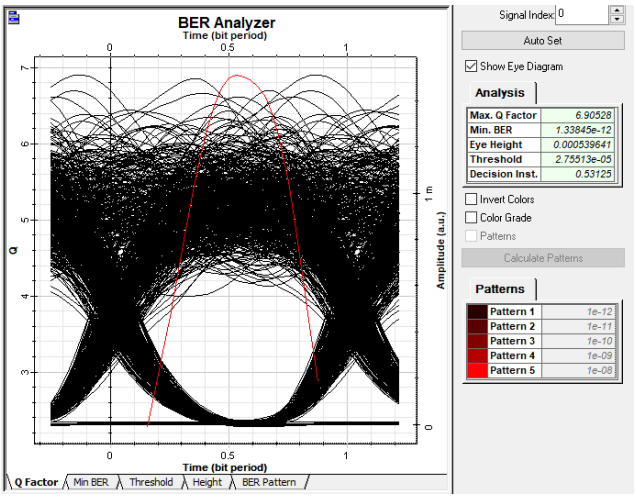

FIGURE 12. Eye diagram obtained for Rx1 from opti-system.

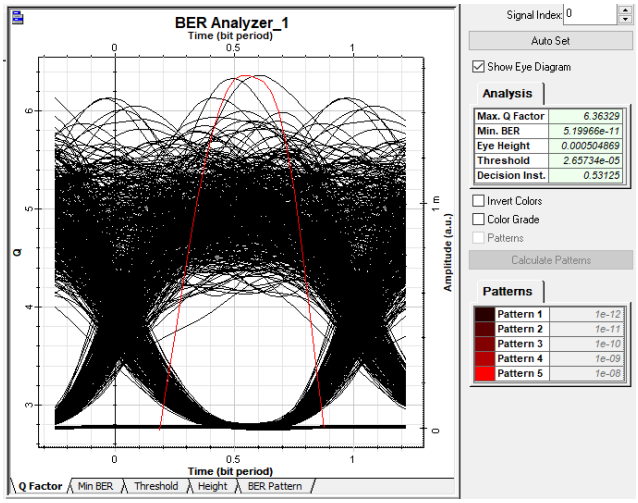

FIGURE 13. Eye diagram obtained for Rx2 from opti-system.

signal, is also higher for Rx1. Overall, this simulation demonstrates that the communication between Tx1 and Rx1 outperforms Tx2 and Rx2 communication. By leveraging the eye diagram and relevant parameters, designers can optimize the location coordinates of the transmitters and receivers of the NeoCommLight system, ensuring reliable and efficient data transmission.

V. IMPLEMENTATION OF NEOCOMMLIGHT SYSTEM

The NeoCommLight system is implemented with one transmitter and one receiver. The VLC receiver picks up the square pulse signal generated by the VLC transmitter. To assess the system's performance, the output of the VLC receiver is fed into an oscilloscope and compared with the signal originating from the VLC transmitter as shown in figure 14. An OTOROYS PowerLED panel of 24 V, 42 W was used for the transmitter, and a Hamamatsu S5973 Pin photodiode was used for the receiver. This experiment was able to transmit data at 800 Kbps at a distance of 200 cm. Increasing the transmission frequency reduces the illumination of the LED panel. This is because the LED panel must turn on and off at a faster rate at higher frequencies. At high frequencies, the transmitter is not able to send a VLC signal over long distances, and the signal becomes distorted. The experiment involved testing the bit rate range from 200 bps to 4 Mbps with a transmission distance of 200 cm. Due to the proportional diminishing of light intensity with distance, an optical concentrator is employed at the receiver. The optical concentrator was added to the receiver to extend the range of the VLC communication system beyond 20 cm to 200 cm. In the low bit rate range, from 200 bps to 100 Kbps, the received signal closely resembled the transmitted signal. However, beyond the bit rate range of 100 Kbps, the received signal began to distort significantly. Despite this limitation, the VLC prototype demonstrated superior performance, with a maximum range of 200 cm between the transmitter and receiver. At this distance, the VLC prototype successfully detected a 600 kHz (1.2 Mbps) signal. For shorter distances, such as within 5cm, the VLC system excelled at transmitting a 1.5 MHz (3 Mbps) signal. By understanding the system's limitations and strengths at different frequencies and distances, we can optimize the VLC circuit design, ensuring reliable and high-speed data transmission.

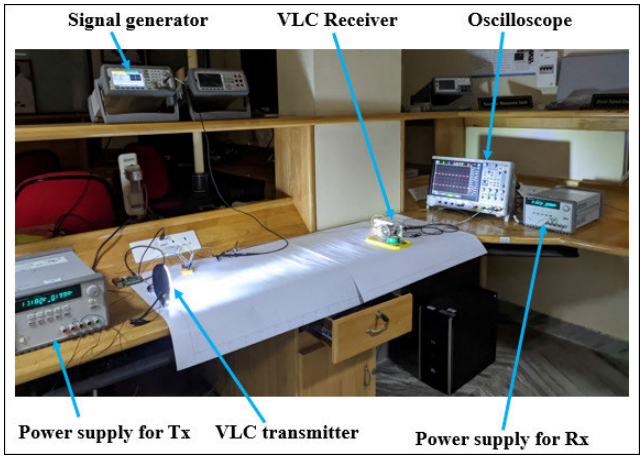

FIGURE 14. Designed prototype of VLC transmitter and receiver.

VI. PERFORMANCE EVALUATION OF NEOCOMMLIGHT SYSTEM

The performance evaluation of the prototype of the NeoCommLight system is performed considering the characteristics such as the variability of the distance between the transmitter (Tx) and receiver (Rx), the communication latency, the average voltage of the received signal, the transmitted source angle, the peak-to-peak voltage of the received signal, transmission bit rate, diffraction angle in case of knife edge obstacle, and so on. These characteristics were carefully assessed to ensure a more satisfactory operation of the system.

A. DELAY PERCENTAGE (%) VS. TRANSMISSION SIGNAL BIT RATE (KBPS) ANALYSIS

Furthermore, we conducted an analysis involving the calculation of the bit-period-to-delay ratio expressed as a percentage. This ratio was pivotal in assessing the relationship between the communication delay and the inherent bit period. Subsequently, the communication latencies or delays (measured in nanoseconds) were translated into delay percentages using the formulation outlined in equation (13). It is imperative to emphasize that delay is not solely contingent on bit rate but is also intrinsically linked to the bit period.

$$Delay\ Precentage = \frac{Delay(ns) \times 100\%}{Bit\ period} \tag{13}$$

The resultant plot, depicted in figure 15, briefly portrays the relationship between the delay percentage of received signals and the bit rate. As the bit rate escalates, the delay percentage in received signals concurrently increases. This trend becomes particularly pronounced when bit rates surpass 200 Kbps. This surge in delay percentage is attributed to the notable discrepancy between high-frequency delays (measured in nanoseconds) and their corresponding bit periods (also measured in nanoseconds).It can be inferred that the transmitter has a maximum bit rate that can be detected at the receiver based on the distance provided. Beyond that maximum bit rate, the receiver is unable to detect the transmitted data for a fixed transmitter-receiver distance. This is the reason why the plotted curves are truncated at some point and beyond that there are no values.

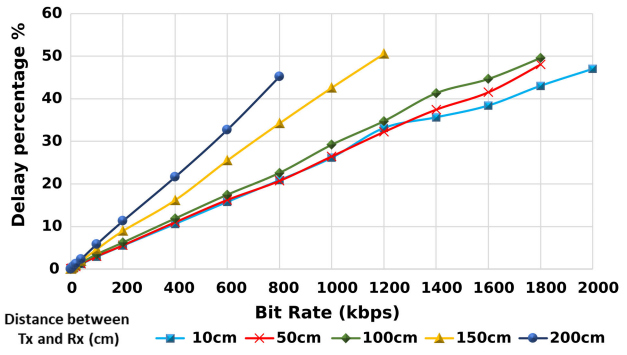

FIGURE 15. Delay percentage(%) - transmission signal bit rate (Kbps) graph.

B. PHASE DIFFERENCE BETWEEN TX AND RX VS. TRANSMISSION SIGNAL BIT RATE ANALYSIS

The phase angle exhibited notable fluctuations in correspondence with both bit rate and distance variations during our experiments in the NeoCommLight prototype. The phase difference quantified in degrees varied between transmitted and received signals, was gauged by the oscilloscope in the prototype. Figure 16, illustrates the phase difference between the transmitter (Tx) and receiver (Rx) against the bit rate. Notably, an increase in bit rate corresponds to an augmented phase difference. This phase shift signifies the angular offset experienced by the received signal. Furthermore, the phase difference increases as an increase in the distance between Tx and Rx while maintaining the same bit rate. The behavior of the delay percentage (%) vs. bit rate (Kbps) plot and the phase difference (degrees) between Tx and Rx vs. bit rate (Kbps) plot are similar.

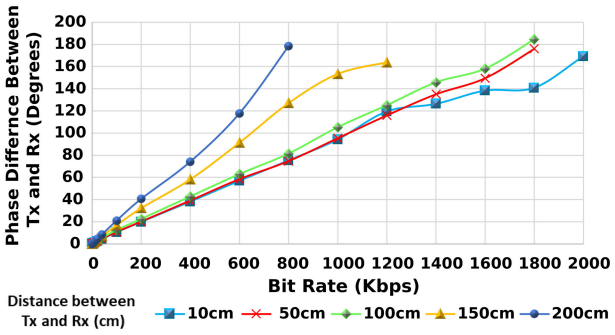

FIGURE 16. Phase difference(degrees) between Tx and Rx VS transmission signal bit rate (Kbps) graph.

C. ILLUMINANCE (LUX) VS. TRANSMISSION SIGNAL BIT RATE (KBPS) ANALYSIS

The experiment to analyze the variations of illuminance with transmission signal frequency (bit rate) was performed without any obstacles between the VLC transmitter and receiver. The VLC transmitter was given bit rate ranging from 200 bps to 2 Mbps, and the lux meter measured the illuminance at the VLC receiver. The variations of the illumination with the transmission bit rate are plotted in figure 17. At shorter distances, the illumination at the receiver side is significantly high. However, by increasing the bit rate while keeping the distance constant, the illuminance diminishes proportionally with the bit rate rise. At elevated frequencies, the transmitted LED necessitates more frequent on-off cycles, contributing to the reduction in illumination observed at the higher frequency ranges. At a greater distance of 50-100 cm, illumination variation was lower compared to 1-40 cm. When the illuminance at the receiving side of the NeoCommLIght prototype is higher, the VLC receiver can efficiently and precisely decipher the transmitted signal. Particularly at lower frequencies (bit rates), when illumination levels are elevated, the NeoCommLight system excels in executing the communication process with efficacy.

D. CONTACT ANGLE (DEGREES) OF THE TRANSMITTER VS. AVERAGE VOLTAGE OF RECEIVED SIGNAL (MV) ANALYSIS

The transmission angle is one of the crucial parameters for realizing the bounds of the NeoCommLight prototype system. Figure 18 illustrates the procedure for measuring the transmission angle concerning the line of sight (LOS) path between Tx and Rx. The transmitter undergoes rotation

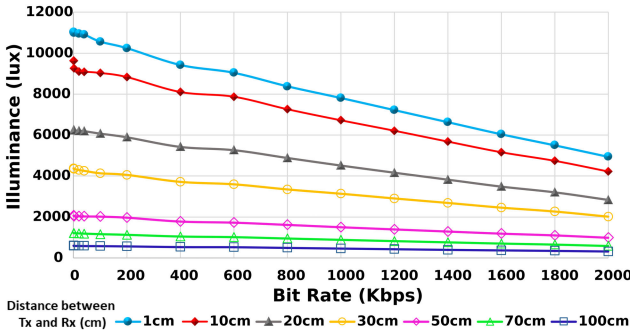

FIGURE 17. Illuminance (lux) versus transmission signal bit rate (Kbps) graph.

both in the anti-clockwise direction, $-\theta$ and in the clockwise direction, $+\theta$. This experiment centered around a range of transmission angles from -35 degrees to $+35$ degrees. The correlation between the transmitting angle and the average voltage of the receiving signal is illustrated in figure 19. The average voltage at the VLC receiver significantly varies when the VLC transmitter alters its angle from the line of sight position.

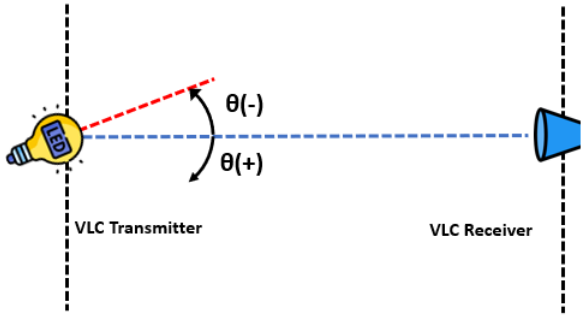

FIGURE 18. VLC transmitter rotation procedure.

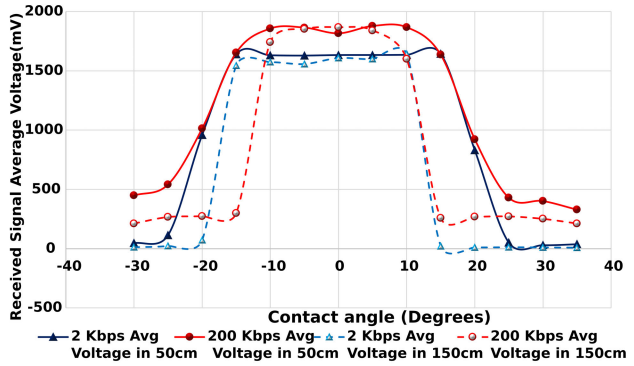

FIGURE 19. Contact angle (degrees) of the Tx - average voltage of received signal (mV) analysis graph.

When the angle was between -15 and $+15$ degrees, an increase in the average voltage of the received signal is observed. According to our observations, the transmitter circuit of the NeoCommLight system has the potential to successfully transmit a signal at an angle between -15 degrees and 15 degrees from the line of sight. The average voltage of the received signal at a distance of 50 cm is greater than the received signal at a distance of 150 cm. The bell-shaped plots in figure 19 reach their highest average voltage values when the transmitting angle is zero degrees ie, at the line of sight.

E. DIFFRACTION ANGLE (DEGREES) VS. TRANSMITTER-OBSTACLE DISTANCE

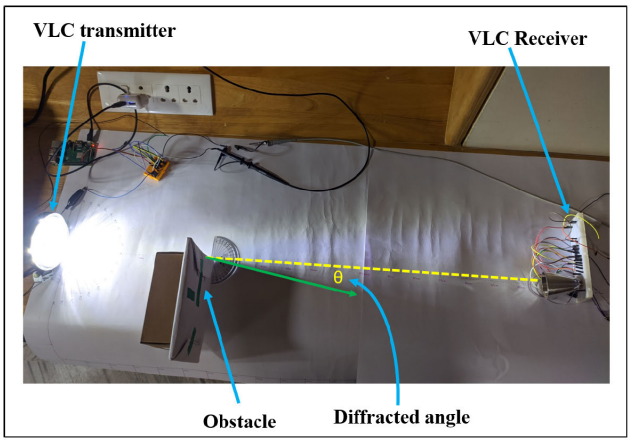

FIGURE 20. Diffraction angle (degrees) of the light in VLC system.

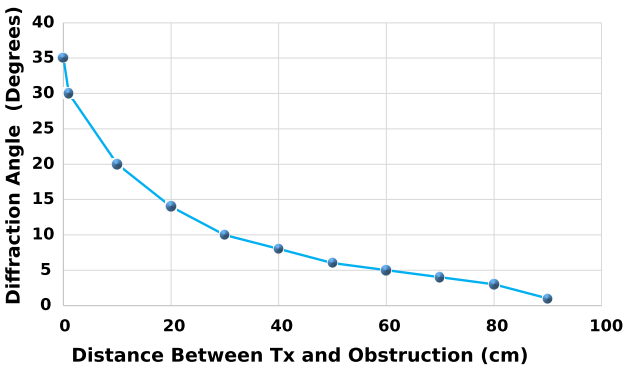

FIGURE 21. Diffraction angle (degrees) with the change of the transmitter-obstacle distance graph.

Since the light signal could not penetrate through the solid object, the shadowing effect becomes one of the significant problems in VLC. The VLC receiver will not be able to decode the transmitted data if the obstacle in between the transmitter and receiver completely blocks (covers 100%) the VLC transmission. In this experiment, we selected a solid object with dimensions, 20 × 20x1 cm^3, and the VLC Tx and Rx were separated by 100 cm. We obstructed the 50% of VLC transmission using the solid object and moved the object between the transmitter and receiver within the 100 cm range. We observed that the light beam undergoes diffraction

after inserting the obstruction between the VLC transmission. It has been shown in figure 20 that due to diffraction the light bends slightly as it passes through the edge of the object. The diffraction angle will change while the obstacle moves between the VLC transmission path. At the receiver side, the average voltage of the received signal was measured using the oscilloscope. Table 6 shows the received signal voltage with the varying transmitter to obstacle distances. In real-world situations, light communication occurs in three dimensions. This experiment was conducted horizontally, as this is easier to demonstrate the diffraction effect. Due to the shorter distance of communication, the horizontal or vertical alignment will not have a significant impact. Low average received signal voltages were obtained when the obstacle was at a distance ranging from 1 cm to 40 cm from the transmitter. When the obstacle was placed in the range of 50 cm to 80 cm, the average received voltage obtained was 1.6 V, which is the same value we obtained without the obstacle. This indicates that when the obstacle with 50% obstruction was positioned between 50 cm to 80 cm from the transmitter, then the obstruction does not affect VLC communication. In the prototype experiment design, the maximum distance for signal reception is tested for 2 meters. The line of sight distance from the ceiling to the NICU unit is approximately 2 meters or less. The reflected signal is definitely more than 2 meters away from the receiver. Therefore, the strength of the reflected signal is very low, and at the receiver it is negligible. Moreover, the interference depends on the positioning of the transceivers. Based on the noise power and received power distributions analysis, the transceivers need to be positioned appropriately. As a result, reflection is not a factor in this experiment.

TABLE 6. Variability of average received signal voltage (mV) in the presence of the obstacle.

Transmitter to obstacle distance (cm)	Average received signal voltage (mV)
1	862
10	890
20	884
30	886
40	909
50	1617.5
60	1620
70	1618
80	1531.4

Figure 21 shows the variability of the diffraction angle (degrees) with the change in distance from the obstruction to the transmitter. We observe an exponential reduction in the diffraction angle as the distance between the transmitter and obstruction increases. Additionally, the experiment showed that if the transmitted light bit rate is altered, there is no significant difference in the diffraction angle. Thus it is concluded that there is no correlation between the diffracted angle and the transmitted bit rate. At a certain distance, the diffraction angle becomes zero, indicating that obstruction does not affect visible light communication.

F. SUMMARY

Aiming at the problem of wireless communication in the RF restricted NICUs, the NeoCommLight system is designed and a prototype has been developed. The performance analysis of the prototype has been presented in this paper which illustrates the interference analysis of the NeoCommLight system, the variability of the parameters of the received VLC signals concerning the illuminance variations, communication latency, delay percentage, phase difference, contact angle of the transmitter and diffraction angle. The system's performance analysis showed that it could transmit data up to 3 Mbps within a two-meter range. Then the following summarizes the interpretations of the performance analysis:

1) The NeoCommLight prototype could transmit a signal with a bandwidth of 800 Kbps at a maximum distance of 200 cm. In addition to this, the prototype could transmit the data with a data rate of 3 Mbps at a distance of 5 cm from the receiver.
2) As the transmission bit rate increases, the delay percentage in the received signals linearly increases. This trend becomes prominent when the transmission signal bit rates surpass 200 Kbps.
3) The phase difference between the transmitted and received signal increases with an increase in the Tx-Rx distance while maintaining the same bit rate.
4) At lower transmission bit rates, the illuminance is higher, and thereby the receiving efficiency of the NeoCommLight system is also high compared to the higher transmission bit rates.
5) When the transmitter contact angle is between -15 and $+15$ degrees, we observed an increase in the average voltage of the received signal.
6) When the obstacle is placed in the range of 50 cm to 80 cm from the transmitter, the average received voltage obtained is 1.6 V, which is the same value we obtained without the obstacle. When the obstacle is between 1 cm and 40 cm from the transmitter, low average signal voltages are received at the VLC receiver.
7) The diffraction angle (due to the placement of the obstacle between the transmitter and receiver) decreases exponentially as the distance between the transmitter and the obstacle increases.
8) There are no significant changes in the diffraction angle concerning the change in the bit rate of the transmitted light.

VII. CONCLUSION

In this paper, we presented the design and architecture of a Visible light communication system, NeoCommLight for RF-restricted NICUs, which is a promising indoor communication method and allows for leveraging the existing lighting infrastructures in the NICUs. The novel architectures were designed for the RF-restricted NICU areas to meet the requirements for the scenarios that would ensue. In the NICU areas with RF restrictions, architecture 1 (One-to-One VLC

communication) is deemed the most reliable architecture, whereas architecture 2 (One Tx and Four Rx) is deemed the most cost-effective method. Since we are dealing with medical data, it is quite significant to model the interference of the system. The mathematically modeled system interference has been analyzed using Optisystem and its results are presented in the paper. The implementation details of the NeoCommLight prototype are described in detail in the paper. The performance analysis of the NeoCommLight prototype illustrated the variations of received signal bit rate with different factors such as delay, distance, illuminance, received power, and angle between the transmitter and receiver. The results obtained are crucial to improving the performance of the NeoCommLight system under different lighting conditions in the NICU.

ACKNOWLEDGMENT

The authors express their deep gratitude to their beloved Chancellor, Sri. Mata Amritanandamayi Devi (AMMA) and faculty and staff members for their support and motivation toward all their endeavors.

REFERENCES

[1] (Oct. 28, 2022). *Does RF Radiation Cause Cancer: American Cancer Society*. The American Cancer Society Medical and Editorial Content Team. [Online]. Available: https://www.cancer.org/healthy/cancer-causes/radiation-exposure/radiofrequency-radiation.html

[2] S. Rehman, S. Ullah, P. Chong, S. Yongchareon, and D. Komosny, "Visible light communication: A system perspective—Overview and challenges," *Sensors*, vol. 19, no. 5, p. 1153, Mar. 2019, doi: 10.3390/s19051153.

[3] B. Donmez, R. Mitra, and F. Miramirkhani, "Channel modeling and characterization for VLC-based medical body sensor networks: Trends and challenges," *IEEE Access*, vol. 9, pp. 153401–153419, 2021.

[4] J. An and W.-Y. Chung, "Single-LED multichannel optical transmission with SCMA for long range health information monitoring," *J. Lightw. Technol.*, vol. 36, no. 23, pp. 5470–5480, Dec. 2018.

[5] G. Shi, Y. Li, and W. Cheng, "Accuracy analysis of indoor visible light communication localization system based on received signal strength in non-line-of-sight environments by using least squares method," *Opt. Eng.*, vol. 58, no. 5, May 2019, Art. no. 056102.

[6] Z. Zhu, Y. Yang, C. Guo, C. Feng, and B. Jia, "Visible light communication assisted perspective circle and arc algorithm for indoor positioning," in *Proc. IEEE Int. Conf. Commun.*, May 2022, pp. 3832–3837.

[7] S. Shen, S. Li, and H. Steendam, "Simultaneous position and orientation estimation for visible light systems with multiple LEDs and multiple PDs," *IEEE J. Sel. Areas Commun.*, vol. 38, no. 8, pp. 1866–1879, Aug. 2020.

[8] H. Haas, L. Yin, C. Chen, S. Videv, D. Parol, E. Poves, H. Alshaer, and M. S. Islim, "Introduction to indoor networking concepts and challenges in LiFi," *J. Opt. Commun. Netw.*, vol. 12, no. 2, pp. A190–A203, Feb. 2020.

[9] M. Lu, F. Wang, R. Li, P. Sun, and Y. Zhang, "Physical layer security for indoor GSM VLC," *Digit. Signal Process.*, vol. 132, Jan. 2023, Art. no. 103824.

[10] H. B. Eldeeb, S. M. Sait, and M. Uysal, "Visible light communication for connected vehicles: How to achieve the omnidirectional coverage?" *IEEE Access*, vol. 9, pp. 103885–103905, 2021.

[11] H. Marshoud, P. C. Sofotasios, S. Muhaidat, and G. K. Karagiannidis, "Multi-user techniques in visible light communications: A survey," in *Proc. Int. Conf. Adv. Commun. Syst. Inf. Secur. (ACOSIS)*, Oct. 2016, pp. 1–6.

[12] J. A. Apolo, S. R. Teli, C. Guerra-Yánez, V. Almenar, B. Ortega, and S. Zvánovec, "Asymmetric hybrid full-duplex POF-based VLC transmission links," *Optik*, vol. 278, May 2023, Art. no. 170701.

[13] J. Davis, Y.-H. Hsieh, and H.-C. Lee, "Humans perceive flicker artifacts at 500 hz," *Sci. Rep.*, vol. 5, no. 1, p. 7861, Feb. 2015, doi: 10.1038/srep07861.

[14] M. Almutairi, L. A. Gabralla, S. Abubakar, and H. Chiroma, "Detecting elderly behaviors based on deep learning for healthcare: Recent advances, methods, real-world applications and challenges," *IEEE Access*, vol. 10, pp. 69802–69821, 2022.

[15] G. D. H. Niranga, V. S. Nair, and S. S. N. B, "Design of a secured medical data access management using Ethereum smart contracts, truffle suite and Web3," in *Proc. 20th ACM Conf. Embedded Netw. Sensor Syst.*, Nov. 2022, pp. 1215–1221, doi: 10.1145/3560905.3568180.

[16] R. Darniss, V. S. Nair, S. S. Nb, and A. R. Devidas, "An IoT based vitals monitoring system for babies in neonatal intensive care unit," in *Proc. IEEE 10th Region 10 Humanitarian Technol. Conf. (R10-HTC)*, Sep. 2022, pp. 130–135.

[17] J. Semmlow, *Circuits, Signals, and Systems for Bioengineers: A MATLAB-Based Introduction*. New York, NY, USA: Academic, 2018, pp. 3–50, doi: 10.1016/B978-0-12-809395-5.00001-1. [Online]. Available: https://www.sciencedirect.com/science/article/pii/B9780128093955000011

[18] H. Wu and Q. Fan, "Study on LED visible light communication channel model based on Poisson stochastic network theory," in *Proc. Int. Conf. Wireless Commun. Smart Grid (ICWCSG)*, Qingdao, China, Jun. 2020, pp. 5–9, doi: 10.1109/ICWCSG50807.2020.00009.

[19] H. Abuella, M. Elamassie, M. Uysal, Z. Xu, E. Serpedin, K. A. Qaraqe, and S. Ekin, "Hybrid RF/VLC systems: A comprehensive survey on network topologies, performance analyses, applications, and future directions," *IEEE Access*, vol. 9, pp. 160402–160436, 2021.

[20] K. M. V. D. Zwaag, M. P. Marinho, W. D. S. Costa, F. De Assis Souza Dos Santos, T. F. Bastos-Filho, H. R. O. Rocha, M. E. V. Segatto, and J. A. L. Silva, "A Manchester-OOK visible light communication system for patient monitoring in intensive care units," *IEEE Access*, vol. 9, pp. 104217–104226, 2021.

[21] A. Makvandi, Y. S. Kavian, and E. Namjoo, "Experimental demonstration of hidden node problem in visible light communication networks," *J. Opt. Commun. Netw.*, vol. 14, no. 9, pp. 691–701, Sep. 2022.

[22] M. K. Jha, N. Kumar, and Y. V. S. Lakshmi, "Performance analysis of transmission techniques for multi-user optical MIMO pre-coding for indoor visible light communication," in *Proc. Int. Conf. Wireless Commun., Signal Process. Netw. (WiSPNET)*, Mar. 2017, pp. 1794–1798.

[23] K. Bhavya, N. Gangrade, and N. Kumar, "Simplified integration of power line and visible light communication," in *Proc. 3rd Int. Conf. Commun. Electron. Syst. (ICCES)*, Oct. 2018, pp. 129–132.

[24] M. K. Jha, N. Kumar, and Y. V. S. Lakshmi, "NOMA MIMO visible light communication with ZF-SIC and MMSE-SIC," in *Proc. 2nd PhD Colloq. Ethically Driven Innov. Technol. Soc. (PhD EDITS)*, Nov. 2020, pp. 1–2.

[25] M. K. Jha, N. Kumar, and Y. V. S. Lakshmi, "Generalized spatial modulation for multi-user in visible light communication," in *Proc. 28th Wireless Opt. Commun. Conf. (WOCC)*, May 2019, pp. 1–5.

[26] M. K. Jha, N. Kumar, and Y. V. S. Lakshmi, "Transmission techniques for multi user MIMO VLC systems using flip-OFDM," *J. Commun.*, vol. 17, no. 6, pp. 452–462, 2022.

[27] T. Tang, T. Shang, and Q. Li, "Impact of multiple shadows on visible light communication channel," *IEEE Commun. Lett.*, vol. 25, no. 2, pp. 513–517, Feb. 2021.

[28] P. Pradeep, P. Divya, R. D. A. Devi, P. Rekha, K. Sangeeth, and M. V. Ramesh, "A remote triggered wireless sensor network testbed," in *Proc. Wireless Telecommun. Symp. (WTS)*, Apr. 2015, pp. 1–7.

[29] M. Katz and D. O'Brien, "Exploiting novel concepts for visible light communications: From light-based IoT to living surfaces," *Optik*, vol. 195, Oct. 2019, Art. no. 163176.

[30] S. Yahia, Y. Meraihi, A. Ramdane-Cherif, A. B. Gabis, D. Acheli, and H. Guan, "A survey of channel modeling techniques for visible light communications," *J. Netw. Comput. Appl.*, vol. 194, Nov. 2021, Art. no. 103206.

[31] F. A. B. Merdan, S. P. Thiagarajah, and K. Dambul, "Non-line of sight visible light communications: A technical and application based survey," *Optik*, vol. 259, Jun. 2022, Art. no. 168982.

[32] Z. Ghassemlooy, W. Popoola, and S. Rajbhandari, *Optical Wireless Communications: System and Channel Modelling With MATLAB*. Boca Raton, FL, USA: CRC Press, 2019.

[33] S. Sancheti, A. Dhaka, A. Nandal, H. G. Rosales, D. Koundal, F. E. L. Monteagudo, C. E. G. Tajada, and A. K. Sharma, "Lambertian luminous intensity radiation pattern analysis in OLOS indoor propagation for better connectivity," *Wireless Commun. Mobile Comput.*, vol. 2022, pp. 1–11, Feb. 2022.

[34] I. M. Abou-Shehada, A. F. AlMuallim, A. K. AlFaqeh, A. H. Muqaibel, K.-H. Park, and M.-S. Alouini, "Accurate indoor visible light positioning using a modified pathloss model with sparse fingerprints," *J. Lightw. Technol.*, vol. 39, no. 20, pp. 6487–6497, Oct. 2021.
[35] Y. Yin, P. Tang, B. Liu, J. Zhang, L. Xia, and B. Liu, "The comparison and analysis of different noise models for visible light communication," in *Proc. Int. Conf. Frontiers Electron., Inf. Comput. Technol.*, May 2021, pp. 1–6.
[36] B. Tipper. (Jun. 15, 2021). *Webinar: Lifi Channel Characteristics*. Optiwave. [Online]. Available: https://optiwave.com/resources/webinars/webinar-lifi-channel-characteristics/
[37] A. Poulose, "Simulation of an indoor visible light communication system using optisystem," *Signals*, vol. 3, no. 4, pp. 765–793, Nov. 2022.
[38] K. Sindhubala and B. Vijayalakshmi, "Design and performance analysis of visible light communication system through simulation," in *Proc. Int. Conf. Comput. Commun. Technol. (ICCCT)*, Feb. 2015, pp. 215–220.
[39] *Si Pin Photodiode S5973: Hamamatsu Photonics*. Si PIN photodiode S5973 | Hamamatsu Photonics. Accessed: Apr. 21, 2023. [Online]. Available: https://www.hamamatsu.com/jp/en/product/optical-sensors/photodiodes/si-photodiodes/S5973.html
[40] *OPA380*. OPA380 Data Sheet, Product Information and Support | TI.com. Accessed: Apr. 21, 2023. [Online]. Available: https://www.ti.com/product/OPA380
[41] *What Is Lambert's Cosine Law (Laws Illumination)*. Tutorials Point. Accessed: Apr. 20, 2023. [Online]. Available: https://www.tutorialspoint.com/what-is-lambert-s-cosine-law-laws-ofillumination
[42] L. Qiao, "An algorithm to reconstruct the constellations based on the superposed character in the multi-dimensional transmission VLC system," *Opt. Commun.*, vol. 534, May 2023, Art. no. 129315.

G. D. HESHAN NIRANGA received the B.Sc. degree in electronics and telecommunication from Sri Lanka Technological Campus, Sri Lanka, in 2020, and the M.Tech. degree in wireless networks and applications from Amrita Vishwa Vidyapeetham, Amritapuri Campus, Kerala, India, in 2023. From March 2019 to September 2019, he was an Intern as a Network Engineer with Hutchison Lanka Pvt. Ltd., Sri Lanka. From May 2021 to November 2021, he was an Assistant Engineer FTTX with Browns Engineering Pvt. Ltd., Sri Lanka. Previously, he published research papers on blockchain and wireless networks in IEEE and ACM conferences. His research interests include visible light communication, optical communication, wireless communication, machine learning, channel modeling, the IoT, blockchain, and embedded systems.

ARYADEVI REMANIDEVI DEVIDAS received the Ph.D. degree in hybrid communication architectures for smart distribution grids. She is currently a Professor (Sl. Gd.) and leads the Intelligent Infrastructure Group, Amrita Center for Wireless Networks and Applications, Amrita Vishwa Vidyapeetham, India. Her research interests include wireless communication, visible light communication, the IoT systems, sensor networks, smart water distribution networks, smart grids, and communication architectures for smart grids. She was an active member of the Indo-European Collaborative Project on Energy Research in Smart Energy Grids named Stabilize-E. She was involved in designing India's first Remote Triggered Laboratory in the area of computer science.

MANEESHA VINODINI RAMESH (Senior Member, IEEE) received the Ph.D. degree in computer science from Amrita Vishwa Vidyapeetham, India. She is currently the Provost of Amrita Vishwa Vidyapeetham and holds multiple portfolios, including Strategic Initiatives, Research and Innovation, Interdisciplinary, and AI+X. She is also the Dean of the International Programs and the School for Sustainable Development, and a Professor and the Director of the Amrita Center for Wireless Networks and Applications. Her extensive work in landslide disaster management has brought accolades to Amrita Vishwa Vidyapeetham. The International Program on Landslides has declared Amrita as the "World Center of Excellence on Landslide Disaster Risk Reduction 2020–2023" at their World Landslide Forum, Kyoto, Japan. In the last couple of years, 2020 and 2021, Stanford University, USA, has ranked her as one of the global top 2% scientists in the networking and telecommunication field for the quality of her research. Her work in multidisciplinary areas, such as the Internet of Things, wireless networks, wireless sensor networks, ML and AI, and sustainable development, successfully applied to thematic areas, such as disaster management, water sustainability, healthcare applications, energy sustainability, and education access. She has provided a direct contribution to societal development.